NANO · MICRO small
www.small-journal.com

Probing Bidirectional Plasmon-Plasmon Coupling-Induced Hot Charge Carriers in Dual Plasmonic Au/CuS Nanocrystals

Patrick Bessel, André Niebur, Daniel Kranz, Jannika Lauth, and Dirk Dorfs**

Heterostructured Au/CuS nanocrystals (NCs) exhibit localized surface plasmon resonance (LSPR) centered at two different wavelengths (551 and 1051 nm) with a slight broadening compared to respective homostructured Au and CuS NC spectra. By applying ultrafast transient absorption spectroscopy we show that a resonant excitation at the respective LSPR maxima of the heterostructured Au/CuS NCs leads to the characteristic hot charge carrier relaxation associated with both LSPRs in both cases. A comparison of the dual plasmonic heterostructure with a colloidal mixture of homostructured Au and CuS NCs shows that the coupled dual plasmonic interaction is only active in the heterostructured Au/CuS NCs. By investigating the charge carrier dynamics of the process, we find that the observed interaction is faster than phononic or thermal processes (< 100 fs). The relaxation of the generated hot charge carriers is faster for heterostructured nanocrystals and indicates that the interaction occurs as an energy transfer (we propose Landau damping or interaction via LSPR beat oscillations as possible mechanisms) or charge carrier transfer between both materials. Our results strengthen the understanding of multiplasmonic interactions in heterostructured Au/CuS NCs and will significantly advance applications where these interactions are essential, such as catalytic reactions.

1. Introduction

Localized surface plasmon resonance (LSPR) is a phenomenon well described for nanocrystals (NCs) of different—typically metallic—materials. LSPR is the resonant excitation of a collective oscillation of the free charge carrier density with the incident light.[1,2] The wavelength of an LSPR mainly depends on the density and effective masses of the free charge carriers as well as on the permittivity of the surrounding medium.[1] By influencing these quantities, the spectral position of the resonance can be controlled, for example via doping,[3] size and shape control,[4,5] shell growth[6] or redox chemistry.[7] Scientific studies on the combination of two plasmonic materials are emerging approaches as an alternative to tune the LSPR, and also to study LSPR interactions.[8–10] When combining two plasmonic materials with a similar LSPR frequency in heterostructured NCs, typically a combined LSPR band centered between the LSPRs of the respective single material component NCs is obtained.[11] If the resonance frequencies of the two materials are sufficiently far apart, two separate LSPRs will be apparent in the combined heterostructure.[8,9,12] A prominent heterostructure system are gold and copper selenide ($Cu_{2-x}Se$, berzelianite) core–shell NCs, in which the resulting gold LSPR is centered in the visible wavelength range (578 nm) and the $Cu_{2-x}Se$ LSPR is centered at near infrared wavelengths (996 nm).[8] Such a system is of particular interest, since the LSPR in $Cu_{2-x}Se$ is based on the collective oscillation of holes. Possible interactions between the two LSPRs can be investigated by conventional steady-state spectroscopy (UV–Vis–NIR absorption), which yields information about the spectral position and broadening of the corresponding absorption band. However, with a lifetime of a few femtoseconds, LSPR is a short-lived process.[5,13,14] The study of its temporal evolution or the temporal evolution of plasmon-induced hot charge carriers is therefore essential to draw conclusions about the underlying processes in a dual plasmonic system.

Generally, LSPR dephases within a few femtoseconds leading to a non-equilibrium distribution of the excited charge carriers.[13,15] Charge carrier scattering (thermalization) within 100 fs results in a Fermi distribution referred to as hot electrons or hot holes, no longer considered plasmons.[16] The hot charge

P. Bessel, A. Niebur, D. Kranz, J. Lauth, D. Dorfs
Institute of Physical Chemistry and Electrochemistry
Leibniz Universität Hannover
D-30167 Hannover, Germany
E-mail: jannika.lauth@uni-tuebingen.de; dirk.dorfs@pci.uni-hannover.de
P. Bessel, D. Kranz, J. Lauth, D. Dorfs
Laboratory of Nano and Quantum Engineering
Leibniz Universität Hannover
D-30167 Hannover, Germany
A. Niebur, J. Lauth, D. Dorfs
Cluster of Excellence PhoenixD (Photonics, Optics and Engineering – Innovation Across Disciplines)
D-30167 Hannover, Germany
J. Lauth
Institute of Physical and Theoretical Chemistry
University of Tübingen
Auf der Morgenstelle 18, D-72076 Tübingen, Germany
The ORCID identification number(s) for the author(s) of this article can be found under https://doi.org/10.1002/smll.202206379.

DOI: 10.1002/smll.202206379

carriers can subsequently undergo scattering with phonons on a timescale of 1–10 ps followed by a final relaxation by heat dissipation (phonon–phonon scattering) within a few hundred picoseconds.[14,15] A transfer of energy rich, hot charge carriers to molecules on the surface or domains of other materials during the relaxation is possible if the energy levels of the excited charge carriers and the receiving material are aligned.[15,17] This transfer gets more efficient with a smaller radius of the NCs, due to the scattering of the charge carriers with the surface, known as Landau damping.[18] In our investigated Au/CuS NC system, a cross excitation of gold and copper sulfide LSPRs is indicated by a transient change of the optical properties operational in both directions. This interaction also leads to small, but unspecific changes in the steady-state spectroscopy.[8,9]

Heterostructured NCs represent a combination of different materials in a single NC and exhibit an excellent opportunity to combine properties of the different material combinations and to investigate interactions.[19] Dual plasmonic NCs with a spectral separation of both LSPRs like the Au/CuS system studied here have been synthesized successfully previously.[9,20] However, the interactions between both domains and their transient optical changes have not been described yet since research on cross-interactions in dual plasmonic systems are still at an early stage. For example, Shan et al. have synthesized Au@$Cu_{2-x}Se$ nanocrescents and performed transient absorption spectroscopy (TAS) with a non-resonant excitation at 380 and 800 nm to investigate the underlying charge carrier interactions between the Au and $Cu_{2-x}Se$ NCs and the different optical properties of the heterostructured NCs.[8]

Here, we investigate synthesized dual plasmonic Au/CuS NCs with TAS to gain insight into cross-interactions between the Au electron LSPR at UV–Vis wavelengths and the CuS hole LSPR at near-infrared (NIR) wavelengths. The respective LSPRs are excited resonantly either at 551 (2.25 eV) or 1051 nm (1.18 eV) and are probed with a low intensity white-light continuum covering 350 to 1400 nm (3.54–0.89 eV). The transient response is followed up to 300 ps after excitation and compared to the reference systems of homostructured Au NCs, CuS NCs, and a mixture of Au and CuS NCs. Strikingly we find a typical hot charge carrier relaxation at LSPR wavelengths of both materials regardless of which LSPR is excited resonantly and conclude, that energy and/or charge carrier transfer between both materials occurs, since the observed effect is faster than phononic or thermal processes. This is the first time that such a type of interaction is observed and will help to deepen the understanding of interactions in dual plasmonic nanomaterials.

2. Results and Discussion

Figure 1A–D shows TEM images of the synthesized pure Au NCs and CuS NCs, respectively, as well as heterostructured Au/CuS NCs. Heterostructured Au/CuS NCs exhibit a diameter of 19.6 nm ± 2.6 nm and a quasi-spherical Au core with a diameter of 9.4 nm ± 2.6 nm (N = 250). With 83.4% the majority of NCs is heterostructured (N = 350). The remaining NCs are either pure CuS NCs (16.3%) or pure Au NCs (0.3%). The results are expected, as the heterogeneous nucleation is energetically preferred to the homogeneous nucleation in general.[22] The synthesized heterostructured Au/CuS NCs are Janus particles, the Au cores are not fully enclosed by the CuS shell. In the mixture (Figure 1D) consisting of pure Au NCs and pure CuS NCs used for our spectroscopic investigations, the Au NCs exhibit a diameter of 9.4 nm ± 2.2 nm and the CuS NCs have a diameter of 11.2 nm ± 1.4 nm. The mixture is composed of 50% CuS NCs and 50% Au NCs, heterostructured NCs are not found by TEM analysis (N = 350). All NCs are clearly separated from each other (see Figure S1, Supporting Information, for the size distributions). The molar Cu:Au ratio is 1.6 in the heterostructured NCs and 1 in the NC mixture determined with atomic absorption spectroscopy (AAS). X-ray diffraction patterns are shown in Figure S2, Supporting Information, for the pure NCs, the heterostructured NCs and the NC mixture and match the reflections of elementary gold (PDF Card # 01-071-3755) and covellite (PDF Card # 00-006-0464) with minor impurities. The reflections are broadened as expected for nanomaterials. UV–Vis–NIR spectra of the NC dispersions are shown in Figure 1E: Both, the pure Au (yellow) and CuS NCs (blue) exhibit a single LSPR band with a maximum at 525 and 1067 nm, respectively. The heterostructured Au/CuS NCs (red) exhibit two maxima of the LSPR bands centered at 551 and 1051 nm, respectively. The Au LSPR is bathochromically shifted by 26 nm, probably stemming from the higher permittivity at the Au LSPR frequency of the surrounding inorganic shell. The oscillating excitation during LSPR induces a fast alternating polarization. The response of the surrounding medium (defined by its permittivity ε_m) influences the oscillation of the charge carriers and therefore the LSPR frequency. The permittivity of the different surrounding media is calculated from the refractive index n for Au and CuS via an approximated Sellmeier equation (ε_m (toluene) = 2.38,[23] $\varepsilon_{m,\ 551\,nm}$ (covellite) $\approx n^2_{551\,nm} \approx 2.54^2 \approx 6.4$ [24]).[1] In contrast, the CuS LSPR is hypsochromically shifted by 16 nm, which is likewise explained by a change in permittivity of the surrounding medium, as the permittivity of gold ($\varepsilon_{m,\,1051\,nm}$ (gold) $\approx n^2_{1051\,nm} \approx 0.272^2 \approx 0.073$ [25]) is lower than the permittivity of toluene.[1] Similar trends are found in other recent works.[8,9]

To underpin if an interaction in Au and CuS NCs is only possible with a shared interface (like in the heterostructured Au/CuS NCs), a mixture of Au and CuS NCs is prepared for comparison with a similar ratio of extinction at the LSPR maxima in steady-state absorption as the heterostructured Au/CuS NCs. The LSPR maxima of the NC mixture are located at 525 and 1067 nm, respectively, and indicate that the pure NCs are not interacting with each other in the mixture. We derive the concentrations of Au and Cu from AAS, the molar extinction coefficients are then calculated using the Beer–Lambert law. The extinction coefficient of the heterostructured Au/CuS NCs are lower than the values of the pure Au and CuS NCs or the mixture, matching previous reported results.[8] All dispersions are stable over several months when stored under inert conditions and show no changes in the UV–Vis–NIR spectra within this time period.

In order to gain information on the interactions between both LSPRs we use TAS. Heterostructured Au/CuS NCs are photoexcited resonantly at the maximum of the Au or the CuS plasmon at 551 (2.25 eV) or 1051 nm (1.18 eV), respectively. The monoplasmonic systems and the mixture are used as a

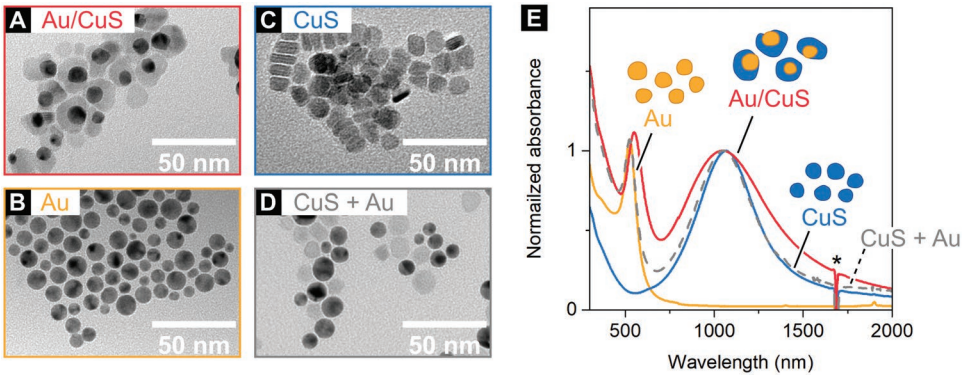

Figure 1. A–D) TEM bright field images of A) heterostructured Au/CuS NCs, B) pure Au NCs, C) pure CuS NCs, and D) a mixture of Au and CuS NCs. E) Normalized absorbance spectra of the respective NCs dispersed in toluene. The spectra are normalized to the maxima of the CuS LSPR, except for the pure Au NCs which are normalized to have the same extinction as the Au LSPR of the NC mixture. *The sharp signal at 1685 nm originates from the baseline correction of the first harmonic of the aromatic C—H vibration absorption of toluene.[21]

reference, on which the same TAS measurements are performed. We do not find any transient response for a non-resonant excitation of pure Au NCs at 1051 nm and pure CuS NCs at 551 nm as is shown in Figure S3, Supporting Information. For the mixture of pure Au and CuS NCs we only observe the transient response of the hot charge carriers stemming from the resonantly excited LSPR, as shown in Figure S4, Supporting Information. This observation is expected, since the absorption maximum of the pure Au NCs coincides with the absorption minimum of the pure CuS NCs and vice versa. When pure Au NCs are resonantly excited at 2.25 eV (551 nm), the typical transient signals are probed and shown in **Figure 2**A. A decaying bleach signal at 2.36 eV (525 nm) is hypsochromically shifted by 3 meV (0.6 nm) with respect to the maximum of the steady-state absorption and exhibits two adjacent induced absorption signals at 2.09 (593 nm) and 2.67 eV (464 nm). 10 ps after excitation, the bleach signal has decayed by 80%. No absorbance change (nor a steady-state absorption) is probed in the NIR region. We observe a similar behavior for the resonant excitation of the CuS NCs at 1.18 eV (1051 nm) as shown Figure 2B. Like in Au NCs, a resonant photoexcitation of the CuS NCs causes a decaying bleach signal at 1.09 eV (1137 nm), with an adjacent induced absorption signal in the visible range at 2.34 eV (529 nm). We expect a second induced absorption signal below 1 eV, since the adjacent positive signals are caused by the broadening of the absorption band.[26]

By following the evolution of the transient signals over time, insights are gained into the processes described above (dephasing, thermalization, charge carrier–phonon scattering, and phonon–phonon scattering). However, the dephasing and charge carrier thermalization step cannot be observed directly here because of temporal resolution restraints. First, the generated laser pulses have a pulse duration of 100 fs and the instrument response function (IRF) for the measurements is limited to ≈150 fs. Second, the pulses propagate through 2 mm of toluene containing the NCs. Therefore, the pulses experience chromatic dispersion of toluene, which leads to an additional loss of temporal resolution, especially when probed in the visible range and pumped in the NIR (1.18 eV).[27] The cooling processes of plasmon-induced hot electrons and hot holes however exhibit time constants between several 100 fs and several 100 ps and can therefore be followed nicely by the measurement. For the analysis of the TAS measurements, we use that the measured ΔA data is the difference of the excited absorption A^* and the ground state absorption A_0. Our fitting procedure is presented for the simplest case: the resonant excitation of pure Au NCs and is applied to all other cases subsequently. The spectral slices are fitted as the difference of two Gaussian curves representing A^* and A_0, as shown in **Figure 3**A.

The data is well described by this approach, even though interband transitions occur at higher energies, which are visible above 3.0 eV (e.g., transition 5d to 6sp band with 3.1 eV, in general >2.4 eV)[28] in the steady-state absorption spectra in Figure 1E. We assume that these interband transitions are not excited by the pump pulse or that possible changes are significantly faster than the IRF of our measurement (150 to 350 fs) as we find no transient signals indicative for these transitions. The measured ΔA spectrum is exclusively induced by the presence of hot charge carriers and the associated decrease of charge carriers in the ground state levels. The vanishing of the absorption change over time is caused by the relaxation of the hot charge carriers to the ground state. This is taken into account by keeping A_0 fixed over time and recalculating A^* for each time step, as shown in Figure S5, Supporting Information. As ΔA approaches zero over time, the excited state A^* also converges into the ground state A_0. This fitting procedure provides the time evolution of the amplitude (Amp), the broadening and the energetic position after excitation, which all approach the respective ground state parameters, see Figure 3B–D. The progression of the fit parameters, with the non-excited absorbance displayed in brown and the evolving excited state absorbance in yellow, respectively. Further conclusions are drawn from the fit parameters by applying the Drude model, which is commonly used to analyze LSPRs bands in steady-state spectroscopy:[1]

$$\omega_{sp} = \sqrt{\frac{\omega_p^2}{\varepsilon_\infty + 2\varepsilon_m} - \gamma^2} \tag{1}$$

where ω_{sp} is the LSPR frequency, ω_p is the bulk plasma frequency, ε_∞ is the relative permittivity at high frequencies (ε_∞ (Au) = 1.53,[29] ε_∞ (CuS) = 8.4[30]), ε_m is the relative permittivity of the surrounding medium, that is, toluene (ε_m = 2.38[23]),

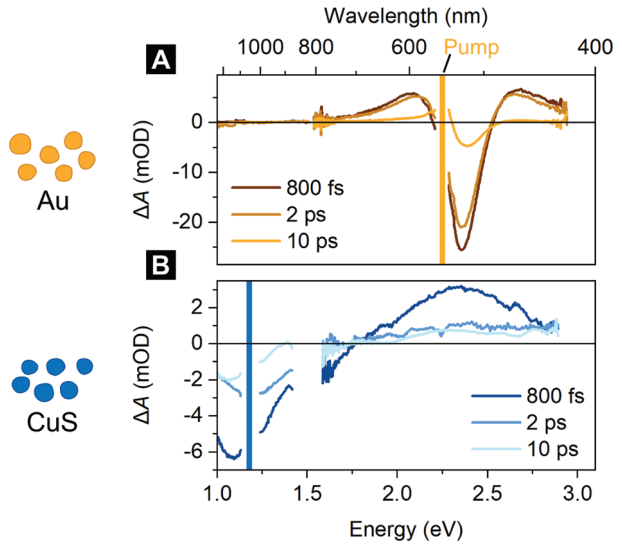

Figure 2. TAS spectral slices at 800 fs, 2 ps, and 10 ps after resonant excitation of A) pure Au NCs (yellow) and B) pure CuS NCs (blue) dispersed in toluene. Vertical colored lines are wavelengths of the pump pulses at 2.25 (551 nm) and 1.18 eV (1051 nm), respectively.

and γ is the damping factor determining the linewidth (FWHM) of the LSPR.[1] The frequency of the plasmon ω_p is equal to:

$$\omega_p = \sqrt{\frac{Nq_e^2}{\varepsilon_0 m_{eff}}} \tag{2}$$

where N is the density of the charge carriers, q_e is the elementary charge, ε_0 is the vacuum permittivity, and m_{eff} is the effective mass of the respective charge carriers.[1] By substituting this expression into Equation (1) and transforming it, an expression for the ratio of the density of the charge carriers and their effective mass N/m_{eff} is obtained:

$$\frac{N}{m_{eff}} = \frac{\left(\omega_{sp}^2 + \gamma^2\right)\left(\varepsilon_\infty + 2\varepsilon_m\right)\varepsilon_0}{q_e^2} \tag{3}$$

The expression for N (Equation (3) multiplied by m_{eff}) is commonly applied to LSPR bands by assuming a constant m_{eff}.[13] For TAS measurements, however, a constant effective mass of the charge carriers cannot be assumed, as the electronic structure is drastically altered by the pump pulse. An expression for N/m_{eff} takes into account that a change of both the charge carrier density and the effective mass determine

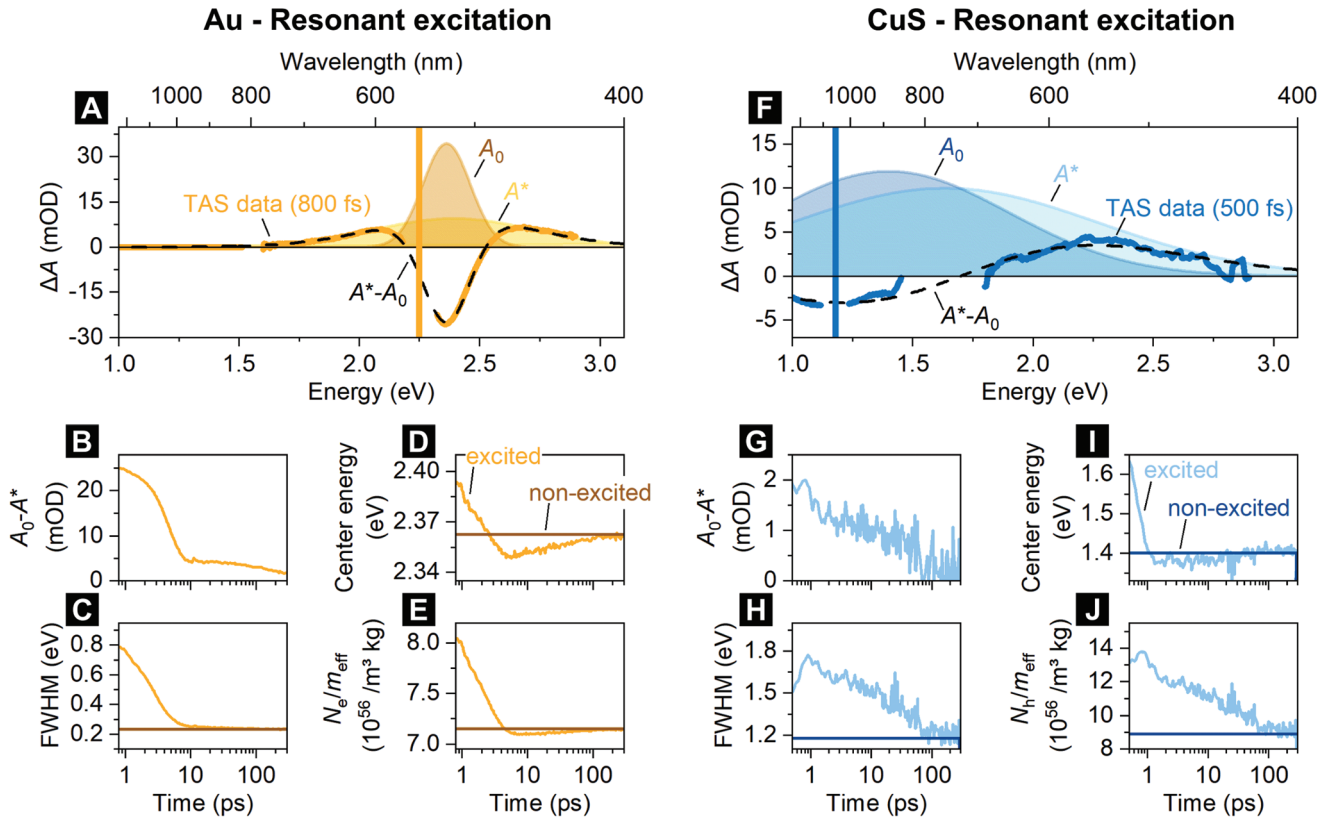

Figure 3. A) TAS of resonantly excited Au NCs after 800 fs. The dotted line indicates the fitted data as a difference of the excited and a non-excited contribution (A^*, yellow and A_0, brown, respectively). B–D) Fitted amplitude, FWHM, and center energy plotted versus time after the excitation. E) Charge carrier density over effective charge carrier mass versus the time derived from the fitted parameters. F) TAS of resonantly excited CuS NCs after 500 fs fitted analogously to panel (A). G–J) Fitted and derived parameters versus time after excitation for resonantly excited CuS NCs: amplitude, FWHM, and center energy, charge carrier density over effective charge carrier mass.

Table 1. Time constants of the amplitude, center energy, FWHM, and N/m_{eff} fitted by bi-exponential decays, derived from resonantly excited Au NCs and CuS NCs, respectively.

	Pure Au NCs		Pure CuS NCs	
Analyzed parameter	τ_{fast} [ps]	τ_{slow} [ps]	τ_{fast} [ps]	τ_{slow} [ps]
Amplitude	*	215 ± 25	0.8 ± 0.2	63 ± 11
Center energy	1.43 ± 0.03	30 ± 2	0.27 ± 0.02	26 ± 7
FWHM	2.26 ± 0.02	32 ± 3	4.7 ± 2.3	53 ± 8
N/m_{eff}	1.60 ± 0.02	20 ± 2	1.4 ± 0.3	49 ± 6

*This fast decay process doesn't follow an exponential decay.

the respective LSPR.[1,31] In all derived data (amplitude, energetic position, broadening, and N/m_{eff}), shown in Figure 3B–E, from the TA signals of the pure Au and CuS NCs, we find two mono-exponential decay contributions before the ground state is reached again. This corresponds to a fast electron–phonon scattering process and a slower phonon–phonon scattering process, as summarized in **Table 1**. Except for the amplitude, all parameters are well described by such bi-exponential decay dynamics, representing electron–phonon scattering and phonon–phonon scattering, respectively. The fitted kinetics are shown in Figure S6, Supporting Information.

For resonantly excited Au NCs we assign the faster relaxation process of N/m_{eff} with a time constant of 1.60 ± 0.02 ps to carrier–phonon and the slower process with 20 ± 2 ps to phonon–phonon scattering. These values are in good agreement with previously reported time constants measured with TAS (2.5 ps, and >50 ps).[14] Measurements and data evaluation of resonantly excited CuS NCs are shown in Figure 3F–J. The fitting procedure of CuS NCs is less accurate compared to the Au NCs because the TAS measurement spans the full available spectral range and one of the two induced absorption signals cannot be mapped due to the probing range limit at 1600 nm. Therefore, relatively strict boundary conditions were set for the fitting of the first time step, as summarized in Table S1, Supporting Information. We find that A^* shifts via two processes associated with fast hole–phonon scattering and slow phonon–phonon scattering with time constants of 270 ± 20 fs and 26 ± 7 ps, respectively. The time constant of carrier–phonon scattering is consistent with literature observations (<1 ps[32]) and is generally faster than in noble metal NCs (1 ps to 4 ps[33]). The remaining parameters of A^* (Amp, FWHM, N/m_{eff}) do not follow a clear two-phase relaxation, which is attributed to the rather low fit quality of the spectral slices. For heterostructured Au/CuS NCs we follow the same procedure by resonantly photoexciting the structures either at the Au or the CuS LSPR band maximum. When exciting resonantly to the energetically higher Au LSPR band maximum (2.25 eV), we observe transient changes both at visible and NIR wavelengths, see **Figure 4**A. In fact, the transient features of pure Au NCs and CuS NCs are found in the ΔA spectrum of the heterostructure Au/CuS NCs when excited at 2.25 eV. This observation implies the presence of hot electrons and holes associated with the high-energy Au LSPR and low-energy CuS LSPR, respectively, and an energy transfer process between the Au and CuS domain. However, interestingly, the same observation is made when the heterostructured Au/CuS NCs are excited resonantly to the CuS LSPR, as shown in Figure 4B.

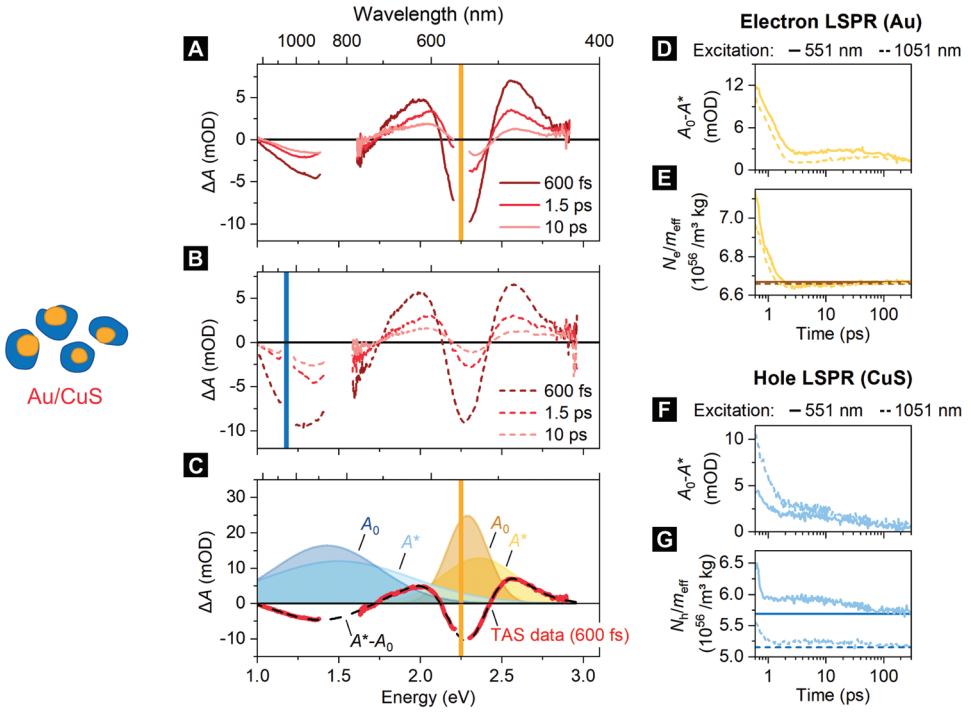

Figure 4. A,B) TAS of heterostructured Au/CuS NCs at 600 fs, 1.5 ps, and 10 ps after excitation with 551 and 1051 nm pulses, respectively. C) Transient absorption of Au/CuS NCs at 600 fs after excitation with a 551 nm pulse. D) Fitted amplitude versus time after excitation corresponding to the electron plasmon. The solid lines represent photoexcitation at 551 nm and the dashed lines 1051 nm. E) Charge carrier density over effective charge carrier mass of the electron plasmon versus time calculated with fitted parameters. F,G) The same as in panels (D) and (E) but for the CuS plasmon.

The energy of the pump pulse (1.18 eV) is not sufficient to directly excite the LSPR of pure Au NCs, as shown in Figure S3A, Supporting Information. Nevertheless, we probe the characteristic transient response of hot electrons in the visible wavelength range. Since we probe transient responses in both energetic regions, the data is fitted using four Gaussians, which represent the excited and ground state absorption, as shown in Figure 4C. We find almost identical decay dynamics regardless which LSPR band in heterostructured Au/CuS NCs is excited resonantly, as is shown for the amplitude and N/m_{eff} for both excitation energies in Figure 4D–G, and for the spectral position and FWHM in Figure S6, Supporting Information. Note that the fitting procedure of the hot electrons (Au domain) leads to decay dynamics that are almost independent of the excitation energy of the pump pulse. Meanwhile, all fitting parameters of the hot holes (CuS domain) have dynamics that are independent of the excitation energy but have constant offsets. Again, these offsets are likely linked to the difficult fitting procedure of the transient signal of the hot holes, being overlayed by the response of the hot electrons in the visible range. Since the decay dynamics of both, the hot electrons and the hot holes are independent of whether the electron plasmon or the hole plasmon is excited, we assume that the same thermalized system is present 600 fs after excitation at 1.18 or 2.25 eV. This implies, that the underlying transfer processes between the Au and CuS domain are faster than the respective IRFs between 150 and 300 fs and are therefore assumed to originate from charge carrier interactions, since both carrier–phonon and phonon–phonon scattering processes are orders of magnitude slower.[15] In contrast the time constant of the decaying hot electrons in pure Au NCs is slower (1.60 ± 0.02 ps) than in the heterostructured NCs (0.36 ± 0.01 ps) indicating a fast charge carrier-based interaction between the Au and the CuS area, which allows the charge carriers generated in the gold to relax partially via the CuS (which exhibits faster carrier–phonon relaxation dynamics). The time constants of the fitted amplitude and N/m_{eff} for both excitation energies are summarized in **Table 2**.

Likewise, a transfer of hot charge carriers to the respective other material is favored by the NC geometry, as in the process of the Landau Damping hot charge carriers are generated directly at the surface of the plasmonic domain.[15] This could be a reason why the time constants of the carrier–phonon scattering (e.g., in N/m_{eff}) from the electron and hole LSPR in the heterostructured Au/CuS NCs approach each other more closely. Due to the fact that both domains are in direct contact with each other, the hot charge carriers could be transferred to the respective other domain. Thus, when adding a CuS shell around pure Au NCs, the electron–phonon scattering is significantly accelerated. Another possible effect resulting in a dual plasmonic interaction could be caused by LSPR beat oscillations, an interference effect of two similar (but not equal) LSPR frequencies resulting in a beat frequency of $\omega_{beat} = |\omega_2 - \omega_1|$.[34] Since both LSPRs in Au/CuS heterostructured NCs feature broad absorption bands, many oscillation frequencies and hence a resulting broad variety of possible beat frequencies occur. Since a beat oscillation has by definition always a lower frequency than its superimposed oscillations the Au LSPR beat might excite the CuS LSPR directly (the Au LSPR is just about broad enough that a beat with a frequency equal to the low frequency edge of the CuS LSPR could occur). Obviously in the same way the CuS LSPR could excite an Au LSPR beat. Furthermore it would also be possible that an Au LSPR beat excites a CuS LSPR beat or vice versa.

Table 2. Time constants of the amplitude, and N/m_{eff} fitted by bi-exponential decays, derived from heterostructured Au/CuS NCs that are resonantly excited to the Au LSPR (2.25 eV) and the CuS LSPR (1.18 eV) respectively. We assign the underlying processes to electron–phonon scattering (τ_{fast}) and phonon–phonon scattering (τ_{slow}).

		Hot electrons		Hot holes	
Excitation [eV]	Parameter	τ_{fast} [ps]	τ_{slow} [ps]	τ_{fast} [ps]	τ_{slow} [ps]
1.18	Amplitude	0.74 ± 0.02	4.0 ± 0.4	0.45 ± 0.02	32 ± 3
2.25	Amplitude	0.66 ± 0.01	520 ± 40	0.36 ± 0.02	39 ± 4
1.18	N/m_{eff}	0.33 ± 0.01	–	0.11 ± 0.01	40 ± 4
2.25	N/m_{eff}	0.36 ± 0.01	–	0.16 ± 0.01	130 ± 40

3. Conclusion

In this work we synthesized dual plasmonic Au/CuS NCs consisting of Au cores and an asymmetric CuS shell with high yields (83.4%). In steady-state UV–Vis–NIR spectra two LSPRs are visible at 551 (2.25 eV) and 1051 nm (1.18 eV), respectively, and give no clear indication of coupling between both LSPRs. Using TAS we show that a resonant excitation at either LSPR maximum in the heterostructured Au/CuS NCs leads to a characteristic hot charge carrier relaxation associated with charge carriers stemming from both LSPRs. The almost identical decay dynamics of the hot charge carriers for both excitation energies indicate that 600 fs after exciting the heterostructured NC system, it contains the same hot charge carriers (electrons and holes), regardless of the excitation energy. The energy and/or charge transfer between the two Au and CuS domains is therefore assumedly based on charge carrier interaction, which is faster than the time range for phononic or thermal interactions. As a result, the time constant of the carrier–phonon scattering of Au NCs decreases (1.6 ps in pure Au NCs to 0.33 ps in Au/CuS hetero NCs).

This work presents the first observation of a bidirectional interaction between two LSPRs by transient observation of the hot charge carrier response of both materials. These findings are highly interesting for photocatalytic and hot charge carrier-related applications in general, especially since hot charge carriers are generated here at the Au LSPR frequency with a significantly lower photon energy than needed for a resonant excitation by making use of the dual plasmonic interactions with CuS in the Au/CuS NC heterostructure.

4. Experimental Section

Used Chemicals: Chloroform (99.8%), copper(II)acetylacetonate ($Cu(acac)_2$, 99.99%), 1,2-dichlorobenzene (DCB, 99%), methanol (MeOH, 99.8%), 1-octadecene (ODE, 90%), oleylamine (OLAM, 70%), sulfur (S, 99.98%), and toluene (≥99.5%) were purchased from Sigma Aldrich. Ethanol (EtOH, 99.8%) was purchased from Roth. Hydrogen

tetrachloroaurate(III) trihydrate ($HAuCl_4 \cdot 3\ H_2O$, 99.99%) was purchased from Alfa Aesar. All chemicals were used as received without further purification.

Synthesis of Au NCs: Au NCs were synthesized following a procedure of Sun et al.[20] OLAM (20 mL) were heated to 160 °C while stirring under Ar atmosphere and kept at this temperature for 20 min. A 1 M solution of $HAuCl_4 \cdot 3\ H_2O$ in water (0.4 mL) was added quickly. The reaction was kept at 160 °C for another 60 min and then cooled to room temperature. After adding MeOH (≈20 mL), the reaction solution was centrifuged for 10 min at 10 621 rcf. The nanocrystals were dispersed in DCB (20 mL) for the growth of CuS or toluene (20 mL) for the NC mixture.

Synthesis of Heterostructured Au/CuS NCs: The heterostructured Au/CuS NCs were synthesized following a procedure of Sun et al.[20] $Cu(acac)_2$ (0.4 mmol), OLAM (4 mL), and Au NCs in DCB (20 mL) were heated to 80 °C while stirring. A 0.1 M solution of S in DCB (4 mL) was injected quickly. The solution was heated to 100 °C under Ar atmosphere and kept at that temperature for 30 min. After cooling to room temperature EtOH (≈20 mL) were added and the reaction solution was centrifuged for 20 min at 3773 rcf and the nanocrystals were dispersed in toluene (20 mL). To separate bigger nanocrystals, the dispersion was centrifuged again at 100 rcf for 5 min and the solution decanted.

Synthesis of CuS NCs: The CuS NCs were synthesized following a modified procedure of Sun et al.[20] $Cu(acac)_2$ (0.4 mmol) and OLAM (4 mL) were heated to 80 °C while stirring. A 0.1 M solution of S in DCB (4 mL) was injected quickly. The solution was heated to 100 °C under Ar atmosphere and kept at that temperature for 30 min. After cooling to room temperature EtOH (≈20 mL) were added and the reaction solution was centrifuged for 20 min at 3773 rcf and the nanocrystals were dispersed in Toluene (20 mL).

Preparation of the Au and CuS NC Mixture: 0.465 mL of the Au NC dispersion was added to 0.4 mL of the CuS NC dispersion to obtain the same absorbance amplitudes as measured for the heterostructured Au/CuS NCs.

Optical Spectroscopy: UV–Vis–NIR spectra were collected in transmission mode using a Cary 5000 spectrophotometer by Agilent Technologies. The samples were diluted in toluene and placed in quartz glass cuvettes with 10 mm path length. A gratin and detector change was conducted at 800 nm and a lamp change was conducted at 350 nm.

Transient Absorption Spectroscopy: Samples were prepared as colloidal solutions in toluene in quartz glass cuvettes with a 2 mm pathway and were constantly stirred in order to prevent laser mediated phase transitions or decomposition.[35] Ultrafast charge carrier dynamics were studied by broadband pump-probe spectroscopy in a set-up described previously and briefly discussed here.[36] 100 fs laser pulses with a wavelength of 800 nm were generated by a Ti:sapphire amplifier system (Spectra-Physics, Spitfire ACE) and split in order to get pump and probe (90:10) pulses. The pump beam wavelength was adjustable from 300 to 1600 nm by nonlinear frequency mixing in an optical parametric amplifier and second harmonics generation system (TOPAS, Lightconversion). To ensure comparable TA measurements, all samples were excited at a pump fluence of 150 µJ cm^{-2}. At this photon flux, the transient signals behave linearly, so that two-photon processes were ruled out, as shown in Figure S7, Supporting Information. The probe pulse was converted to a broadband supercontinuum using nonlinear processes in a CaF_2 or sapphire crystal, allowing probing from 320 to 1600 nm (Ultrafast Systems, Helios FIRE). The probe pulse could be delayed up to 8 ns after photoexcitation via an automatic delay line. Pump and probe pulse pass the cuvette with a maximum overlap. After transmission, the probe pulse was measured by a fiber-coupled detector array at different delay times to follow ultrafast processes causing changes in the absorption.

Electron Microscopy: TEM images were obtained using a FEI Tecnai G2 F20 device equipped with a field emission gun. The acceleration voltage was 200 kV. The samples were washed by precipitation with EtOH and centrifugation. The nanocrystals were dispersed in chloroform and 20 µL of this dispersion were dropcasted on a 300 mesh Cu grid by Quantifoil.

Atomic Absorption Spectroscopy: The gold and copper concentrations of the NC dispersions were determined by AAS using a Varian AA 140 spectrometer. Aliquots of the dispersions were taken and the solvent was completely evaporated. Subsequently, the residual solid was dissolved in freshly prepared aqua regia. These solutions were diluted with deionized water. The extinctions in the atomic absorption spectrometer were measured in relation to separately prepared calibration standards with known copper and golds mass concentration.

Supporting Information

Supporting Information is available from the Wiley Online Library or from the author.

Acknowledgements

P.B. and A.N. contributed equally to this work. The authors would like to thank Armin Feldhoff for providing the XRD facility. P.B. is grateful for being funded by the Hannover School for Nanotechnology (HSN). D.D. thanks the Deutsche Forschungsgemeinschaft for the DFG Research Grant 1580/5-1. D.D. and J.L. are thankful for funding by the Deutsche Forschungsgemeinschaft (DFG, German Research Foundation) under Germany's Excellence Strategy within the Cluster of Excellence PhoenixD (EXC2122, Project ID 390833453) and access to the Ti:sapphire amplifier system (major equipment DFG, Project ID 231415720, Michael Oestreich, Jens Hübner). J.L. is grateful for funding through the Caroline Herschel program of Leibniz Universität Hannover. D.K. is grateful for funding by the Konrad-Adenauer-Stiftung (KAS).

Open access funding enabled and organized by Projekt DEAL.

Conflict of Interest

The authors declare no conflict of interest.

Data Availability Statement

The data that support the findings of this study are available from the corresponding author upon reasonable request.

Keywords

hot charge carrier relaxation, localized surface plasmon resonance (LSPR), localized surface plasmon resonance, transient absorption spectroscopy, ultrafast dynamics

Received: October 17, 2022
Revised: December 15, 2022
Published online: January 15, 2023

[1] A. L. Routzahn, S. L. White, L.-K. Fong, P. K. Jain, *Isr. J. Chem.* **2012**, *52*, 983.
[2] K. L. Kelly, E. Coronado, L. L. Zhao, G. C. Schatz, *J. Phys. Chem. B* **2003**, *107*, 668.
[3] M. Kanehara, H. Koike, T. Yoshinaga, T. Teranishi, *J. Am. Chem. Soc.* **2009**, *131*, 17736.
[4] V. Juvé, M. F. Cardinal, A. Lombardi, A. Crut, P. Maioli, J. Pérez-Juste, L. M. Liz-Marzán, N. Del Fatti, F. Vallée, *Nano Lett.* **2013**, *13*, 2234.

[5] K. Yu, L. Polavarapu, Q.-H. Xu, *J. Phys. Chem. A* **2011**, *115*, 3820.
[6] R. Himstedt, P. Rusch, D. Hinrichs, T. Kodanek, J. Lauth, S. Kinge, L. D. A. Siebbeles, D. Dorfs, *Chem. Mater.* **2017**, *29*, 7371.
[7] A. Wolf, T. Härtling, D. Hinrichs, D. Dorfs, *ChemPhysChem* **2016**, *17*, 717.
[8] B. Shan, Y. Zhao, Y. Li, H. Wang, R. Chen, M. Li, *Chem. Mater.* **2019**, *31*, 9875.
[9] A. Wolf, T. Kodanek, D. Dorfs, *Nanoscale* **2015**, *7*, 19519.
[10] M. Sun, X. Fu, K. Chen, H. Wang, *ACS Appl. Mater. Interfaces* **2020**, *12*, 46146.
[11] R. Borah, S. W. Verbruggen, *J. Phys. Chem. C* **2020**, *124*, 12081.
[12] T. Tsangas, C. Ruhmlieb, S. Hentschel, H. Noei, A. Stierle, T. Kipp, A. Mews, *Chem. Mater.* **2022**, *34*, 1157.
[13] E. Minutella, F. Schulz, H. Lange, *J. Phys. Chem. Lett.* **2017**, *8*, 4925.
[14] T. S. Ahmadi, S. L. Logunov, M. A. El-Sayed, *J. Phys. Chem.* **1996**, *100*, 8053.
[15] A. M. Steiner, F. Lissel, A. Fery, J. Lauth, M. Scheele, *Angew. Chem., Int. Ed.* **2021**, *60*, 1152.
[16] A. Furube, S. Hashimoto, *NPG Asia Mater.* **2017**, *9*, e454.
[17] Y. Zhang, S. He, W. Guo, Y. Hu, J. Huang, J. R. Mulcahy, W. D. Wei, *Chem. Rev.* **2018**, *118*, 2927.
[18] T. V. Shahbazyan, *Phys. Rev. B* **2016**, *94*, 250905.
[19] N. C. Bigall, W. J. Parak, D. Dorfs, *Nano Today* **2012**, *7*, 282.
[20] C. Sun, M. Liu, Y. Zou, J. Wei, J. Jiang, *RSC Adv.* **2016**, *6*, 26374.
[21] L. G. Weyer, *Appl. Spectrosc. Rev.* **1985**, *21*, 1.
[22] N. T. K. Thanh, N. Maclean, S. Mahiddine, *Chem. Rev.* **2014**, *114*, 7610.
[23] G. Ritzoulis, N. Papadopoulos, D. Jannakoudakis, *J. Chem. Eng. Data* **1986**, *31*, 146.
[24] L. Xiao, J. Wu, J. Ran, Y. Liu, W. Qiu, F. Lu, F. Shao, D. Tang, P. Peng, *AIP Adv.* **2016**, *6*, 85122.
[25] D. W. Lynch, W. R. Hunter, in *Handbook of Optical Constants of Solids*, (Ed. E. D. Palik), Academic Press, Burlington **1997**, pp. 275–367.
[26] F. Scotognella, G. Della Valle, A. R. Srimath Kandada, D. Dorfs, M. Zavelani-Rossi, M. Conforti, K. Miszta, A. Comin, K. Korobchevskaya, G. Lanzani, L. Manna, F. Tassone, *Nano Lett.* **2011**, *11*, 4711.
[27] P. Devi, V. V. Lozovoy, M. Dantus, *AIP Adv.* **2011**, *1*, 32166.
[28] a) W. J. Scouler, *Phys. Rev. Lett.* **1967**, *18*, 445; b) L. Schoenlein, E. Fujimoto, *Phys. Rev. Lett.* **1987**, *58*, 1680; c) X. Zhang, C. Huang, M. Wang, P. Huang, X. He, Z. Wei, *Sci. Rep.* **2018**, *8*, 10499.
[29] P. G. Etchegoin, E. C. Le Ru, M. Meyer, *J. Chem. Phys.* **2006**, *125*, 164705.
[30] Y. Xie, W. Chen, G. Bertoni, I. Kriegel, M. Xiong, N. Li, M. Prato, A. Riedinger, A. Sathya, L. Manna, *Chem. Mater.* **2017**, *29*, 1716.
[31] B. A. Mansour, S. E. Demian, H. A. Zayed, *J. Mater. Sci.* **1992**, *3*, 249.
[32] I. Kriegel, C. Jiang, J. Rodríguez-Fernández, R. D. Schaller, D. V. Talapin, E. da Como, J. Feldmann, *J. Am. Chem. Soc.* **2012**, *134*, 1583.
[33] S. Link, M. A. El-Sayed, *Annu. Rev. Phys. Chem.* **2003**, *54*, 331.
[34] X. Zhang, J. He, Y. Wang, F. Liu, *Sci. Rep.* **2016**, *6*, 18902.
[35] a) D. Kranz, P. Bessel, M. Niemeyer, H. Borg, M. Rosebrock, R. Himstedt, N. C. Bigall, D. Dorfs, *J. Phys. Chem. C* **2022**, *126*, 15263; b) M. Niemeyer, P. Bessel, P. Rusch, R. Himstedt, D. Kranz, H. Borg, N. C. Bigall, D. Dorfs, *ChemNanoMat* **2022**, *8*, 2.
[36] a) F. C. M. Spoor, L. T. Kunneman, W. H. Evers, N. Renaud, F. C. Grozema, A. J. Houtepen, L. D. A. Siebbeles, *ACS Nano* **2016**, *10*, 695; b) A. Spreinat, M. M. Dohmen, J. Lüttgens, N. Herrmann, L. F. Klepzig, R. Nißler, S. Weber, F. A. Mann, J. Lauth, S. Kruss, *J. Phys. Chem. C* **2021**, *125*, 18341; c) L. F. Klepzig, L. Biesterfeld, M. Romain, A. Niebur, A. Schlosser, J. Hübner, J. Lauth, *Nanoscale Adv.* **2022**, *4*, 590.